Nonequilibrium heat flows through a nanorod sliding across a surface

Alexander V. Popov, Douglas C. Viehman, and Rigoberto Hernandez

Citation: J. Chem. Phys. **134**, 104703 (2011); doi: 10.1063/1.3561296
View online: http://dx.doi.org/10.1063/1.3561296
View Table of Contents: http://jcp.aip.org/resource/1/JCPSA6/v134/i10
Published by the American Institute of Physics.

Nonequilibrium heat flows through a nanorod sliding across a surface

Alexander V. Popov,[a] Douglas C. Viehman, and Rigoberto Hernandez[b]
Center for Computational and Molecular Science and Technology, School of Chemistry and Biochemistry, Georgia Institute of Technology, Atlanta, Georgia, USA

(Received 29 November 2010; accepted 10 February 2011; published online 8 March 2011)

The temperature-ramped irreversible Langevin equation [A. V. Popov and R. Hernandez, J. Chem. Phys. **134**, 244506 (2007)] has been seen to describe the nonequilibrium atomic oscillations of a nanorod dragged across a surface. The nanorod and surface consist of hydroxylated α-Al_2O_3 layers as was studied earlier by Hase and co-workers [J. Chem. Phys. **122**, 094713 (2005)]. The present approach corresponds to the reduced Frenkel–Kontorova–Tomlinson model in which only one element of the vibrational chain representing a surface layer is considered explicitly. The key new concept centers on a separation of the environment into two effective reduced-dimensional baths: an equilibrium bath arising from the thermostated vibrations of the crystal lattice and a nonequilibrium bath arising from driven oscillations at the contact between the nanorod and the surface. The temperature of the latter is defined by the mean energy of a representative atomic oscillator for a given layer. The temporal temperature fluctuations and the dependence of the static part of the temperature on the sliding velocity are close to those found in the MD simulations of Hase and co-workers. © *2011 American Institute of Physics*. [doi:10.1063/1.3561296]

I. INTRODUCTION

The dynamic friction between two surfaces involves many different aspects such as the specific structure of the interacting solid bodies, interatomic interactions, oscillatory excitations of atoms belonging to adjoining layers, and the energy dissipation due to coupling of these oscillations with the vibrations of the crystal lattice. The phenomenological forms of friction at various length scales have been known for a couple of centuries. Its rigorous treatment remains a theoretical challenge because it creates mismatches between deterministic and nondeterministic approaches that differ depending on the time and length scale of the theoretical framework characterizing it. Many theoretical approaches in tribology resolve this issue by reducing the problem to a single figure of merit at a specific length scale. Among these are the behavior of lubricants,[1–4] properties of different types of surface compositions,[3,5] and the energy dissipation in terms of sliding instabilities which are directly linked to submolecular modes of moving substrates.[6]

The last two decades are filled with many attempts and successes using molecular dynamics (MD) models to simulate frictional processes between different surfaces under various conditions, see Refs. 7–19. Typically these MD simulations are propagated by nondeterministic equations of motion in which effective degrees of freedom are subsumed within a system of Langevin equations (LE).[20] Although stochastic and dissipative forces in these equations are not needed for constructing a strict theory, their role is crucial for the convergence of the simulations involving small (or reduced-particle) systems where the main effect—friction—is directly connected to energy dissipation processes. The purpose of the present article is to demonstrate the equivalence between a simple reduced-dimensional (or coarse-grained) model and an MD simulation in describing the energy transfer across the frictional contact between a surface and a nanoscale object. This therefore serves as an example of how an invariant concept of friction can be retained across disparate scales.

In a series of articles, Hase and co-workers[21–24] have reported the nonequilibrium energy transfer dynamics in MD simulations of a nanoscale object consisting of 13 sublayers of hydroxylated α-Al_2O_3 nanosurfaces sliding across a much larger surface of the same type. To prevent the uncontrolled heating of the system, the outermost layers of both surfaces were connected to thermostats. It was found that the velocity distribution for the atoms—and, therefore, their temperatures—in different layers oscillate during the sliding in accord with the periodicity of the interfacial potential. The temperature amplitudes of the oscillations may reach 1000–3000 K and decrease with the distance from the contacting interfaces. The friction force decreases when the sliding velocity increases. This has been interpreted as a manifestation of the "stick-slip" and "smooth sliding" regimes which depend on whether the atoms have time to relax in their equilibrium positions between two consecutive kicks of the periodic force. Analogous observations have been reported in Refs. 10 and 11 for the first three layers of diamond surfaces. Although all the processes involved in this frictional contact can hardly be presented within one theoretical framework, there are several ongoing attempts to get a clear picture by use of simple mechanical models.

One approach is based on the use of the linear response theory and Green function technique[25,26] to treat the set of oscillators representing a crystal structure. Sokoloff[27] suggested that the horizontal motion (along the sliding direction)

[a]Permanent address: Technological Institute, Kemerovo 650056, Russia.
[b]Author to whom correspondence should be addressed. Electronic mail: hernandez@gatech.edu. Fax: 404-894-0594.

of atoms be described by the use of a system of equations

$$m\ddot{x}_k = F_k(\{x\}, t) - \Gamma\dot{x}_k, \tag{1}$$

for each atom k in a layered compound. In this equation, m is the atomic mass, Γ is the phenomenological damping constant and F_k is the force which consists of the harmonic terms, $-\kappa_k(x_k - x_j)$, between adjacent atoms, and the periodic force, acting on the lowest layer, $-\lambda_0 \sin((2\pi/a)(x_k + ut))$. Here a is the lattice constant in the horizontal x-y plane; u is the sliding velocity; κ_k represents the force constants which differ for atoms belonging to a single layer ($\kappa_k = \alpha$) and to neighboring layers ($\kappa_k = \beta$); and $\lambda_0 = \beta a/2\pi$. The upper layer in this model is constrained to be stationary. Sokoloff claims that this model "incorporates the basic physics of the problem" and is capable of yielding the basic relationships between the outer parameters of the system such as the amplitude of the periodic force and the overall friction force. However, the model does not reveal the proper nonequilibrium observables describing the internal characteristics of the crystal surface. The nonequilibrium behavior originates from the imbalance between the energy pumping (due to the forced sliding) and the energy dissipation (to the thermostats). This leads to nontrivial internal effects. For example, the effective temperature of the atomic layers is not uniform. In summary, approaches based on Eq. (1) presume that the atomic motion is damped within a time scale Γ^{-1}. They are therefore not capable of accounting for nonequilibrium effects such as nonstationary energy redistribution or long-lived fluctuations at longer time scales.

Another approach for analyzing the frictional contact between a nanorod and a surface lies in models based on a stochastic representation of the atomic motion. The *ad hoc* introduction of random forces into Eq. (1) turns it into the form of a Langevin equation. The random terms can be associated with the interactions between atoms and the vibrations of the crystal lattice originating from the equilibrated subsystem, i.e., with phonons spreading along the vertical direction z. Following this idea, we suggest a model which is more elaborated—and yet simpler—than that of Sokoloff. The effects observed in Ref. 24 can be recovered from this single-particle phenomenological equation. The model is based on a class of generalized Langevin equations (GLEs),

$$m\ddot{x} = F(x, t) - \int_0^t g(t)g(t')\gamma(t - t')\dot{x}(t')dt' + R(t), \tag{2}$$

in which the temporal change in the environment response to the chosen coordinate is included through time-dependent coupling coefficients,[28,29] $g(t)$, and the random force, $R(t)$, obeys the relation,

$$\langle R(t)R(t')\rangle = k_B T g(t)g(t')\gamma(t - t'). \tag{3}$$

Here $\gamma(t - t')$ is the friction kernel of the unperturbed system at equilibrium, and the coupling function $g(t)$ strongly depends on the state and structure of the bath. The validity of this sort of irreversible GLE (iGLE) has recently been justified through simulations of nonstationary colloidal suspensions.[30–32] In the stationary limit, the functions $g(t)$ become constant and Eq. (3) acquires the standard from of the fluctuation-dissipation relation (FDR).

In Ref. 32, this method has been extended to include nonstationary temperature effects as well as the interactions with several nonequilibrium baths. (Such approaches in which the environment contains several baths are frequently used to describe nonstationary or glassy systems.[33–36]) The resulting equation of motion as well as the generalized FDR are more complicated than Eq. (2) and not presented here. However, the time scale of the process under investigation is that of the temperature changes of crystal sublayers (bath modes). The latter is slower than the random force correlation function which can be attributed to the atomic oscillations (see Sec. IV for parameters values). In this case, the iGLE approach can be simplified by replacing the friction kernel with a δ-function to obtain the so-called "irreversible" LE (iLE):[28]

$$m\ddot{x} = F(x, t) - \sum_k g_k^2(t)\Gamma_k\dot{x} + \sum_k \sqrt{2k_B T_k(t)g_k(t)\Gamma_k}\,\xi_k(t), \tag{4}$$

where the summation is performed over the bath reservoirs, and the noise terms obey the condition

$$\langle \xi_k(t)\xi_n(t')\rangle = \delta_{kn}\delta(t - t'). \tag{5}$$

The bath reservoirs can have different temperatures, $T_k(t)$, and friction coefficients, Γ_k. In the present work, the lattice structure of the nanorod does not change much as it is being dragged. Consequently, the coefficients $g_k(t)$ are nearly constant and close to unity.

The model central to this work is illustrated in Fig. 1. The interaction of every atom within the ith layer it belongs to (the "horizontal" interaction) is projected onto a single effective particle propagated by a stochastic term and a complementary friction force. The nonstationary temperature $T_i(t)$ of this layer is taken into account in the framework of the modified iLE:

$$m\ddot{x}_i = F_i(x_i, t) - (\Gamma + \Gamma_i)\dot{x}_i + \sqrt{2k_B(\Gamma T + \Gamma_i T_i(t))}\,\xi(t), \tag{6}$$

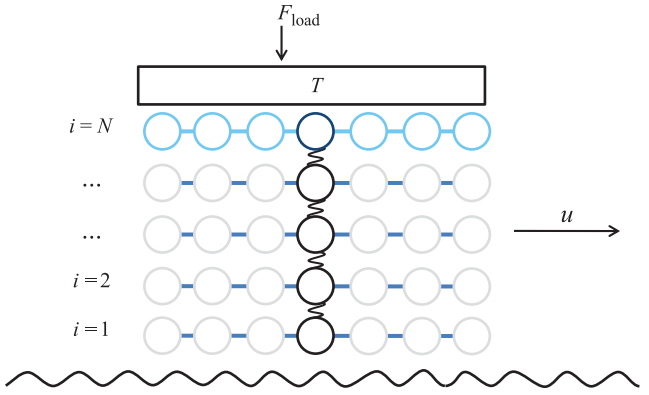

FIG. 1. A schematic representation of a nanorod sliding across a surface of similar hydroxylated $\alpha - Al_2O_3$ layers. As shown, the nanorod is represented by N finite layers. In a perfect crystal, each layer consists primarily of the same atom but that is not differentiated in the diagram though the physical parameters in the corresponding model are correspondingly differentiated. In the reduced dimensional model, each such layer is projected onto a single effective particle (shown in dark black) which interacts through an effective force with the layers below and above. The top layer (shown in blue) is thermalized through its direct contact with an external body applying a loading force F_{load}.

where Γ_i defines the coupling with the local bath consisting of the neighbor atoms of the same layer i. The basic model is described in Sec. II. Various analytical limits of the model are described in Sec. III. A concrete application of this method to the energy dissipation at the interface between a nanorod and a surface as previously explored by Hase and co-workers[21–24] is presented in Sec. IV.

II. STOCHASTIC MODEL

A. A coupled linear spring-bead model (LSBM)

A nanorod is modeled as a layered material consisting of N layers of atoms (see Fig. 1) which is dragged across an averaged, but structured, surface. The nanorod model combines elements from those described in Refs. 24 and 27. The lowest layer, labeled by the index $i = 1$, is assumed to experience periodic interactions at the "washboard" frequency $\omega(u) = 2\pi u/a$ with $a = 2.47$ Å. The top-most layer, labeled by the index $i = N$, is assumed to be in equilibrium due to contact with a stationary bath thermalized at $T = 300$ K. The latter interaction presumably arises from the contact with whatever external agent is dragging the nanorod across the surface. The symmetry of the nanorod across each layer i suggests the appropriateness of representing the dynamics of each layer through a single effective particle self-consistently interacting with a bath of analogous same-layer atoms and the representative particles below and above it at layers $i-1$ and $i+1$, respectively. The motion of this effective particle is characterized by an effective coordinate, x_i, with a corresponding velocity, $v_i = \dot{x}_i$, and an effective mass, m_i. This projection is consistent with the observation in Ref. 23 that the average temperatures T_x, T_y, and T_z are the same for all the layers except the H-atom interfacial layer, where the kinetic energy for the sliding direction is 30–40 K higher than that for other directions. This difference can be neglected if compared with the temperature amplitude which exceeds 1000 K.

We assume that the system of equations of motion for the atomic layers has the following form:

$$m_1\dot{v}_1 = -k_1x_1 - \kappa_{1,2}(x_1 - x_2) + F_1(t) - \Gamma_1^T v_1 - \Gamma_1^E v_1 + \sqrt{2k_BT\Gamma_1^T}\,\xi_1^T(t) + \sqrt{2k_BT_1(E_1)\Gamma_1^E}\,\xi_1^E(t), \quad \text{for } i = 1, \tag{7a}$$

$$m_i\dot{v}_i = -k_ix_i - \kappa_{i,i-1}(x_i - x_{i-1}) - \kappa_{i,i+1}(x_i - x_{i+1}) - \Gamma_i^T v_i - \Gamma_i^E v_i + \sqrt{2k_BT\Gamma_i^T}\,\xi_i^T(t) + \sqrt{2k_BT_i(E_i)\Gamma_i^E}\,\xi_i^E(t), \quad \text{for } i > 1. \tag{7b}$$

Here k_i is the restoring force constant which defines the oscillations of a representative atom within the ith layer and $\kappa_{i,i\pm1}$ are the force constants which are responsible for couplings between the layers. The periodic force $F_1(t)$ acts on the lowest surface layer and depends on the dragging velocity, u. In each equation, Γ_i^T and Γ_i^E are the friction coefficients corresponding to the interactions with the thermalized and local baths which constitute the sources of the stochastic forces represented by two last terms.

The forces $\xi_i^T(t)$ originate from the interactions with the phonons produced by the thermalized bath. In the actual system only the uppermost layer is in direct contact with this bath, and hence these terms would appear only in the equation of motion for layer N. However, the other layers are indirectly connected to this bath with energy fluctuations that would be equilibrated within a time scale connected to the distance of the layer to the uppermost layer and the speed of sound. We therefore include a thermalizing coupling term in the equations of motion of the atoms in every layer instead of considering a hierarchy of sequential perturbations. While this is a gross approximation in the fully elaborated model, the projected (or coarse-grained) model describing each layer with a single effective particle will certainly have such a term, albeit with a possibly different value of the dissipative constants connecting them to the bath at temperature T.

The force $\xi_i^E(t)$ on the effective ith particle is caused by its interaction with atoms in the corresponding ith layer. Each such layer is thereby represented as a thermal bath whose average particle energy E_i defines its effective temperature $T_i(E_i)$. A concrete form of this dependence is discussed in Sec. III. Such a decomposition of the stochastic forces attributed to different subenvironments has been justified in earlier work.[30–32,37] The forces $\xi_i^T(t)$ and $\xi_i^E(t)$ are assumed to be independent standard normal (Gaussian) noise terms each obeying condition (5).

B. Analysis of two-bead LSBM

A special, but illustrative case, arises when the nanorod is only two layers thick. The system of equations (7) reduces to only two equations involving effective particles with coordinates x_1 and x_2 representing two adjacent layers, respectively. Each of the effective particles i is connected to its own local bath with temperature T_i^b. The equations of motion for the particles read

$$m_1\dot{v}_1 = -k_1x_1 - \kappa_{12}(x_1 - x_2) - \Gamma_1 v_1 + \sqrt{2k_BT_1^b\Gamma_1}\,\xi_1(t), \tag{8a}$$

$$m_2\dot{v}_2 = -k_2x_2 - \kappa_{12}(x_2 - x_1) - \Gamma_2 v_2 + \sqrt{2k_BT_2^b\Gamma_2}\,\xi_2(t), \tag{8b}$$

where $\langle\xi_i(t)\xi_j(t')\rangle = \delta_{ij}\delta(t-t')$ and $\langle\xi_i(t)\rangle = 0$.

The energy stored in the system is

$$E = \frac{m_1\langle v_1^2\rangle}{2} + \frac{k_1\langle x_1^2\rangle}{2} + \frac{\kappa_{12}\langle (x_1 - x_2)^2\rangle}{2} + \frac{m_2\langle v_2^2\rangle}{2} + \frac{k_2\langle x_2^2\rangle}{2}. \tag{9}$$

The heat flow from the x_1-layer to x_2-layer is defined by the averaging of the coupling force multiplied by the corresponding velocity as

$$J_{1\to 2} = \kappa_{12}\langle (x_1 - x_2)v_1\rangle. \tag{10}$$

The heat flow in the opposite direction is, by analogy,

$$J_{2\to 1} = -\kappa_{12}\langle (x_1 - x_2)v_2\rangle. \tag{11}$$

The sum of these two flows represent the time derivative of the third (middle) term in Eq. (9).

All the energy terms in expression (9) as well as the heat flows [Eqs. (10)–(11)] can be found through analysis of the second moments. The differential equations for them can be found directly from Eqs. (8) with the help of Itō's lemma which in our case states that for two variables, say, x_1 and v_2, $d(x_1v_2) = x_1dv_2 + v_2dx_1 + dx_1dv_2$. After averaging over the stochastic noise, one obtains ten differential equations. Six of these are

$$\frac{d}{dt}\langle x_1^2\rangle = 2\langle x_1v_1\rangle, \tag{12a}$$

$$\frac{d}{dt}\langle v_1^2\rangle = -2\omega_{01}^2\langle x_1v_1\rangle - 2\gamma_1\left(\langle v_1^2\rangle - k_BT_1^b/m_1\right) - 2\,\Omega_1^2\langle x_1v_1 - x_2v_1\rangle, \tag{12b}$$

$$\frac{d}{dt}\langle x_1v_1\rangle = -\omega_{01}^2\langle x_1^2\rangle - \gamma_1\langle x_1v_1\rangle - \Omega_1^2\langle x_1^2 - x_1x_2\rangle + \langle v_1^2\rangle, \tag{12c}$$

$$\frac{d}{dt}\langle x_1v_2\rangle = \langle v_1v_2\rangle - \omega_{02}^2\langle x_1x_2\rangle - \gamma_2\langle x_1v_2\rangle + \Omega_2^2\langle x_1^2 - x_1x_2\rangle, \tag{12d}$$

$$\frac{d}{dt}\langle x_1x_2\rangle = \langle x_1v_2\rangle + \langle x_2v_1\rangle, \tag{12e}$$

$$\frac{d}{dt}\langle v_1v_2\rangle = -\omega_{01}^2\langle x_1v_2\rangle - \gamma_1\langle v_1v_2\rangle - \Omega_1^2\langle x_1v_2 - x_2v_2\rangle - \omega_{02}^2\langle x_2v_1\rangle - \gamma_2\langle v_1v_2\rangle + \Omega_2^2\langle x_1v_1 - x_2v_1\rangle. \tag{12f}$$

The other four equations can be obtained from Eqs. (12a)–(12d) by permuting indices 1 and 2. In Eqs. (12), $\omega_{0i}^2 = k_i/m_i$, $\Omega_i^2 = \kappa_{12}/m_i$, and $\gamma_i = \Gamma_i/m_i$.

The steady-state regime of the system defined by Eqs. (12) results from equating all the time derivatives to zero and taking into account that averaging over the stochastic noise gives $\langle \xi_i(t)dt\xi_j(t)dt\rangle = \delta_{ij}dt$. In this regime, the mean kinetic energy associated with the temperature T_1 of layer x_1 acquires the form

$$m_1\langle v_1^2\rangle \equiv k_BT_1 = k_BT_1^b + \frac{\gamma_1\Omega_1^2\Omega_2^2k_B\left(T_2^b - T_1^b\right)}{\Delta}, \tag{13}$$

where

$$\Delta = \frac{\gamma_1\gamma_2}{\gamma_1+\gamma_2}\left(\left(\omega_{01}^2 + \Omega_1^2\right) - \left(\omega_{02}^2 + \Omega_2^2\right)\right)^2 + \gamma_1\gamma_2\left(\gamma_1\left(\omega_{02}^2 + \Omega_2^2\right) + \gamma_2\left(\omega_{01}^2 + \Omega_1^2\right)\right) + (\gamma_1+\gamma_2)\Omega_1^2\Omega_2^2. \tag{14}$$

The result for layer x_2 is the permutation of the indices in Eq. (13). The actual temperature T_1 is not equal to the bath reservoir temperature T_1^b and is shifted toward the bath temperature T_2^b of the adjacent layer. Equation (13) and its permuted form for T_2 can be used to renormalize the temperature of the external bath to the one effectively seen within the layer.

The heat flows [Eqs. (10) and (11)] in the steady-state regime can be expressed through the external bath temperatures T_1^b and T_2^b in the usual form. In terms of the actual layer temperatures, however, they read

$$J_{1\to 2} = -J_{2\to 1} = D_{12}\,k_B(T_1 - T_2), \tag{15}$$

with the heat transfer coefficient

$$D_{12} = \frac{(\gamma_1+\gamma_2)\Omega_1^2\Omega_2^2}{\left(\left(\omega_{01}^2 + \Omega_1^2\right) - \left(\omega_{02}^2 + \Omega_2^2\right)\right)^2 + (\gamma_1+\gamma_2)\left(\gamma_1\left(\omega_{02}^2 + \Omega_2^2\right) + \gamma_2\left(\omega_{01}^2 + \Omega_1^2\right)\right)}. \tag{16}$$

For a multilayer system in the stationary regime the heat flow between neighbor layers is constant and always equal to

$$J_{1\to 2} = D_{12}\,k_B(T_1 - T_2) = D_{23}\,k_B(T_2 - T_3) = \cdots = D_{N-1,N}\,k_B(T_{N-1} - T_N), \tag{17}$$

due to energy conservation. Given temperatures at the borders, T_1 and T_N, are predefined, the temperature of any layer k can be found from this equation in the form

$$T_k = \frac{\left(D_{12}^{-1} + \cdots + D_{k-1,k}^{-1}\right)T_N + \left(D_{k,k+1}^{-1} + \cdots + D_{N-1,N}^{-1}\right)T_1}{D_{12}^{-1} + \cdots + D_{N-1,N}^{-1}}. \tag{18}$$

Equations (16) and (18) comprise the central result of this section. According to Eq. (16), only the frequencylike characteristics—namely, the frequencies of atomic vibrations

and their dumping rates—are responsible for the temperature equilibration process. Equation (18) states that there exists a temperature grid which is linear if all the couplings between layers are equal (otherwise, this expression provides the nonlinearity). Thus, the contribution of the uppermost layer temperature, T_N, will be approximately proportional to the distance between the kth and the Nth layers. Note that the profile of the steady-state temperature is fully defined by the relative values of the heat transfer coefficients.

C. Perturbative decoupling of LSBM

Written in a matrix form, Eqs. (7) read

$$\frac{d^2}{dt^2}\hat{\mathbf{M}}\mathbf{X}(t) = -\hat{\mathbf{K}}\mathbf{X}(t)+\hat{\mathbf{K}}'\mathbf{X}(t)+\mathbf{F}(t) - \hat{\mathbf{\Gamma}}\frac{d}{dt}\mathbf{X}(t) + \boldsymbol{\xi}(t), \tag{19}$$

where the vectors and matrices in N-dimensional space are

$$\mathbf{X} = \begin{pmatrix} x_1 \\ \vdots \\ x_N \end{pmatrix}, \quad \mathbf{F} = \begin{pmatrix} F_1(t) \\ 0 \\ \vdots \\ 0 \end{pmatrix}, \quad \boldsymbol{\xi} = \sqrt{2k_{\mathrm{B}}} \begin{pmatrix} \sqrt{T\Gamma_1^T}\,\xi_1^T(t) & + & \sqrt{T_1(E_1)\Gamma_1^E}\,\xi_1^E(t) \\ \sqrt{T\Gamma_2^T}\,\xi_2^T(t) & + & \sqrt{T_2(E_2)\Gamma_2^E}\,\xi_2^E(t) \\ & \vdots & \\ \sqrt{T\Gamma_N^T}\,\xi_N^T(t) & + & \sqrt{T_N(E_N)\Gamma_N^E}\,\xi_N^E(t) \end{pmatrix}, \tag{20a}$$

$$\hat{\mathbf{M}} = \begin{pmatrix} m_1 & & 0 \\ & \ddots & \\ 0 & & m_N \end{pmatrix}, \quad \hat{\mathbf{\Gamma}} = \begin{pmatrix} \Gamma_1^T + \Gamma_1^E & & 0 \\ & \ddots & \\ 0 & & \Gamma_N^T + \Gamma_N^E \end{pmatrix}, \tag{20b}$$

$$\hat{\mathbf{K}} = \begin{pmatrix} k_1 + \kappa_{12} & & & 0 \\ & k_2 + \kappa_{12} + \kappa_{23} & & \\ & & \ddots & \\ 0 & & & k_N + \kappa_{N,N-1} \end{pmatrix}, \quad \hat{\mathbf{K}}' = \begin{pmatrix} 0 & \kappa_{12} & & & 0 \\ \kappa_{12} & 0 & \kappa_{23} & & \\ & \kappa_{23} & \ddots & \ddots & \\ & & \ddots & 0 & \kappa_{N-1,N} \\ 0 & & & \kappa_{N-1,N} & 0 \end{pmatrix}. \tag{20c}$$

The nondiagonal matrix $\hat{\mathbf{K}}'$ is responsible for the coupling between adjacent layers. If it were equal to zero, Eqs. (7) could be decoupled, and each equation would contain the coordinate and velocity of only one layer. To include the effect of the coupling into the system dynamics, plausible perturbative approximations for the nondiagonal terms, $\kappa_i x_{i+1}$ and $\kappa_i x_{i-1}$, can be introduced in the calculation of various correlation functions. After substituting them back into Eqs. (7), decoupled equations are readily obtained and can be solved separately.

To realize the methodology described above, we first find a steady-state solution to Eq. (19) via a Fourier transform,

$$\tilde{\mathbf{X}}(\omega) = [\hat{\mathbf{K}} - \hat{\mathbf{K}}' - \hat{\mathbf{M}}\omega^2 + i\omega\hat{\mathbf{\Gamma}}]^{-1}[\tilde{\mathbf{F}}(\omega) + \tilde{\boldsymbol{\xi}}(\omega)], \tag{21}$$

where $\tilde{f}(\omega) \equiv \int_{-\infty}^{\infty} f(t)e^{i\omega t}dt$ for any function $f(t)$. Averaging over the noise and picking out the coupling operator $\hat{\mathbf{K}}'$ gives

$$\langle\tilde{\mathbf{X}}(\omega)\rangle = [\hat{\mathbf{L}}(\hat{\mathbf{I}} - \hat{\mathbf{L}}^{-1}\hat{\mathbf{K}}')]^{-1}\tilde{\mathbf{F}}(\omega), \tag{22}$$

where

$$\hat{\mathbf{L}} \equiv \hat{\mathbf{K}} - \hat{\mathbf{M}}\omega^2 + i\omega\hat{\mathbf{\Gamma}} \tag{23}$$

is the diagonal matrix describing the nonperturbed dynamics, $\hat{\mathbf{I}}$ is the identity operator and $\langle\cdots\rangle$ denotes the averaging over different realizations of the stochastic force processes.

The washboard frequency, ω, is much smaller than the characteristic vibrational one, $\omega_{0k} = \sqrt{K_{kk}/m_k}$, and the friction coefficient, Γ_{kk}/m_k (the values of parameters for the specific model systems are discussed in Sec. IV). Thus, the operator $\hat{\mathbf{L}}$ in Eq. (23) does not depend on the frequency, and $\hat{\mathbf{L}} \approx \hat{\mathbf{K}}$ with the diagonal elements $L_{kk} \approx K_{kk} = m_k\omega_{0k}^2$. All the averaged coordinates $\langle x_i(t)\rangle$ calculated from Eq. (22) become directly proportional to the force $F_1(t)$.

In this low frequency approximation, Eq. (22) expresses Hooke's law,

$$\langle\tilde{\mathbf{X}}(\omega)\rangle \approx [\hat{\mathbf{K}}(\hat{\mathbf{I}} - \hat{\mathbf{K}}^{-1}\hat{\mathbf{K}}')]^{-1}\tilde{\mathbf{F}}(\omega) = [\hat{\mathbf{K}} - \hat{\mathbf{K}}']^{-1}\tilde{\mathbf{F}}(\omega), \tag{24}$$

i.e., after performing inverse Fourier transform, $\langle x_k(t)\rangle = c_k F_1(t)$ with some constant coefficients c_k. Thus the

averaged (coarse-grained) vibrations of the layers move coherently with the force $F_1(t)$. This is in direct agreement with the observations of Ref. 24 in which the temperatures of the layers are seen to oscillate *synchronously*. It is also notable that all the coefficients c_k are also close to each other and are of the order of the spring constant, κ^{-1}, because the values of the elements of $\hat{\mathbf{K}}$ and $\hat{\mathbf{K}}'$ are close to each other.

We are interested in the terms $\kappa_{k,k\pm1}\langle x_k(t)\rangle$ defining the force with which the neighboring layers act on the kth one. By inspection, these quantities are $\kappa_{k,k\pm1}\langle x_k(t)\rangle = \kappa_{k,k\pm1}c_k F_1(t) = a_{k,k\pm1}F_1(t)$ with $a_{k,k\pm1}$ about unity since $\kappa_{k,k\pm1}c_k \sim 1$.

Assuming the coupling is weak and expanding the RHS of Eq. (22) into a power series over $\hat{\mathbf{K}}'$, one gets

$$\langle\tilde{\mathbf{X}}(\omega)\rangle = [\hat{\mathbf{I}} + \hat{\mathbf{L}}^{-1}\hat{\mathbf{K}}' + (\hat{\mathbf{L}}^{-1}\hat{\mathbf{K}}')^2 + \cdots]\hat{\mathbf{L}}^{-1}\tilde{\mathbf{F}}(\omega). \quad (25)$$

Substituting here all the necessary matrices from Eqs. (20) and accounting only for the second-order correction in Eq. (25), one obtains the first three components of vector $\langle\tilde{\mathbf{X}}\rangle$ after some algebra:

$$\langle\tilde{x}_1(\omega)\rangle \approx \left(1 + \frac{\kappa_{12}^2}{L_{11}L_{22}}\right)\frac{\tilde{F}_1(\omega)}{L_{11}} = a_1\frac{\tilde{F}_1(\omega)}{L_{11}}, \quad (26a)$$

$$\langle\tilde{x}_2(\omega)\rangle \approx \frac{\kappa_{12}}{L_{22}}\frac{\tilde{F}_1(\omega)}{L_{11}} = a_2\frac{\tilde{F}_1(\omega)}{L_{11}}, \quad (26b)$$

$$\langle\tilde{x}_3(\omega)\rangle \approx \frac{\kappa_{12}\kappa_{23}}{L_{22}L_{33}}\frac{\tilde{F}_1(\omega)}{L_{11}} = a_3\frac{\tilde{F}_1(\omega)}{L_{11}}, \quad (26c)$$

where $L_{kk} = K_{kk} - m_k\omega^2 + i\omega\Gamma_{kk}$ are the elements of the diagonal matrix $\hat{\mathbf{L}}$. Note that only these first three terms are nonzero in the second-order approximation: the higher-order expansion is needed to calculate the response of higher layers to the perturbation. If the couplings are weak, the proportionality coefficients a_i decrease for higher layers. If the couplings are strong—i.e., if the constants $\kappa_{i,i\pm1}$ and k_i are of the same order,— the coefficients a_i in Eqs. (26) become close to unity. Although the perturbation theory fails in this case, one can expect analogous values for the coefficients a_i if the matrix operations in Eq. (22) are calculated accurately. Thus, it is reasonable to conclude that the quantities of interest, $\kappa_{i,i\pm1}\langle x_i(t)\rangle$, defining the forces with which the neighboring layers act on the ith layer, are proportional to $F_1(t)$ with the proportionality coefficients close to unity.

Strictly speaking, the phases of the averaged coordinates $\langle x_k(t)\rangle$ change with increasing k due to the imaginary parts of the elements L_{kk}. But this change is small if $\omega \ll m_k\omega_{0k}^2/\Gamma_{kk}$. The phase shift becomes apparent only for layers with $k > m_k\omega_{0k}^2/(\Gamma_{kk}\omega)$ because the elements L_{kk} are consecutively multiplied in the denominators of Eqs. (26). For all 13 sublayers of the nanorod investigated in Sec. IV, this effect is negligible (see the values of parameters in Table I). It is also confirmed by the results of Ref. 24, wherein the temperatures of all the layers change synchronously.

TABLE I. Parameters used to calculate the steady-state temperature, T^*, and its smoothed value, $\overline{T}^*$.

Layer	m(a.u.)	ω_0 (10^{12} s^{-1})	γ (10^{12} s^{-1})	p	u_0 (m/s)
H	1	15.52	7.7	0.942	0.01
O	16	3.88	7.7	0.901	0.01
Al	27	2.987	7.7	0.816	0.01

III. PROJECTION OF LSBM ONTO ONE-MODE ILES

A. Excitation force and environmental temperatures

After linearizing the coupling terms $\kappa_{k,k\pm1}\langle x_k(t)\rangle$ and relating them to the force $F_1(t)$, Eqs. (7) can be decoupled. The resulting equation of motion for the representative atom of each layer reads

$$m_i\dot{v}_i = -K_{ii}x_i + F_i(t) - \Gamma_i^T v_i - \Gamma_i^E v_i + \sqrt{2k_BT\Gamma_i^T}\,\xi_i^T(t) + \sqrt{2k_BT_i(E_i)\Gamma_i^E}\,\xi_i^E(t), \quad (27)$$

where the first term corresponds to the intrinsic vibrations with the frequency $\omega_{0i} = \sqrt{K_{ii}/m_i}$, and $F_i(t)$ has the same form as $F_1(t)$ with a possibly different amplitude for the given layer, i. Specifically, the periodic force $F_i(t)$ is defined as

$$F_i(t) = F_{0i} + F_{1i}\cos[\omega(u)t]. \quad (28)$$

While for $i = 1$, it is caused by the direct interaction with the lower sliding surface, higher layers experience a similar and synchronous influence due to the periodic compression of lower layers. In our model, as was shown above, only the amplitudes F_{0i} and F_{1i} may vary for $i > 1$.

This force has a constant component, F_{0i}, to ensure there is a permanent averaged stress imposed by the load. The value of F_{1i} defines the actual amplitude of atomic oscillations which depend on the load and the sliding velocity u through the frequency $\omega(u)$. When u is small, the amplitudes of the oscillations are wide because the atoms have enough time to take up positions with minimal potential energy. At larger u, the oscillations become smaller. Note that writing the force in the predefined time-dependent form of Eq. (28) implies that a regime of smooth sliding has been established. This is possible only at sufficiently large velocities and, thus, the case of the small values of u should be treated with caution. Hase *et al.* interpret the region $u \approx 20$–50 m/s as a transition between the stick-slip and the smooth sliding regimes.[21,22] The former requires intermolecular forces—and coordinates—to be fully "relaxed" each time atoms jump into new positions. These values of u are in accordance with computer simulations[20] which suggest a transition velocity as $u_{tr} \simeq 10^{-2}\,c$ ($c \sim 1000$ m/s is the speed of sound).

Without loss of generality we assume that $F_{1i} = F_{0i}$ because the absolute value of the force F_{0i} leads only to the constant shift in the equilibrium atomic position, This choice means there are relaxing moments during the sliding when $F_i(t) = 0$.

The goal of introducing the concept of ambient temperature and local random forces is to avoid the description of every particle in the crystal, as it is done in, for instance, Ref. 27. For this purpose, proper averaging should be

performed to correctly define the temperature $T_i(E_i)$ of layer i. It can be written through the kinetic energy as

$$k_B T_i(E_i) = \langle m_i v_i^2 \rangle. \tag{29}$$

On the other hand, equating the local temperature to the full energy of the oscillator,

$$k_B T_i(E_i) = \tfrac{1}{2} m_i \langle v_i^2 \rangle + \tfrac{1}{2} \kappa_i \langle x_i^2 \rangle, \tag{30}$$

implies that the motion in the phase space is strongly entangled: the "kinetic" and the "potential" temperatures are equal to each other. Although Eqs. (29) and (30) are always correct for a system in equilibrium, different parts of a nonstationary system can undergo different equilibration mechanisms. In this regard, we need to consider cases of low and high sliding velocity separately.

Although intuitively clear, definition (29) may not fully correspond to the average thermal energy of a particular layer. This temperature reflects the averaged perturbations in the kinetic energy of the ith layer and is suitable for slow sliding. In this case interatomic forces and atomic positions are always equilibrated ("sticky" regime), so that the atomic coordinates shift mostly synchronously leading to the "concerted" relaxation in the sense that the temperature follows the averaged kinetic energy. The oscillatory behavior of the latter for slow sliding can not be smoothed away by averaging over the stochastic noise.

A good solution for faster sliding is to add a complementary potential energy term to Eq. (29). Evenness of the full energy in this case is a reflection of randomness of the phases of thermal vibrations which allows one to identify the full energy with the ambient temperature[Eq. (30)]. This process of random-phase equilibration should occur at relatively high sliding velocities, when permutations in both kinetic and potential energies heat the local environment equally.

Generalizing the above considerations, we redefine the local temperature in the form

$$k_B T_i(E_i) = \left(1 - \frac{\alpha(u)}{2}\right) m_i \langle v_i^2 \rangle + \frac{\alpha(u)}{2} \kappa_i \langle x_i^2 \rangle, \tag{31}$$

where $\alpha(u)$ reflects the contribution of the potential energy into the local temperature. α changes from 0 at $u = 0$ to 1 at large u, and we assume it obeys a simple rule

$$\alpha(u) = \frac{u}{u_0 + u}, \tag{32}$$

where u_0 defines some threshold value between the "concerted" and random-phase equilibration regimes. The former corresponds to the stick-slip motion and the latter to the smooth sliding. At large values of u permanent intensive excitations lead to the energy equilibration in accordance with Eq. (30). However, if sliding is slow, equilibrium atomic positions gradually follow the slowly changing force and, therefore, only the kinetic part of energy contributes into the local temperature through Eq. (29). The function $\alpha(u)$ helps to connect these two limits, and its role is discussed in Sec. IV. Additivity in the stochastic noise implies that the sum of these terms with different amplitudes can be combined to give

$$A\xi_i^T(t) + B\xi_i^E(t) = \sqrt{A^2 + B^2}\, \xi(t), \tag{33}$$

where $\xi(t)$ is a Gaussian (standard normal) noise with the same correlation function as in Eq. (5).

To simplify the analysis, we incorporate Eq. (33) into Eq. (27) to obtain

$$\dot{v}_i = -\omega_{0i} x_i + f_i(t) - \gamma_i v_i + \sqrt{2\gamma_i \left((1 - p_i) \frac{k_B T}{m_i} + p_i \frac{k_B T_i(E_i)}{m_i} \right)}\, \xi(t), \tag{34}$$

where $f_i(t)$ is the acceleration caused by the force $F_i(t)$, $\gamma_i = (\Gamma_i^T + \Gamma_i^E)/m_i$ is the overall relaxation rate, $p_i \equiv \Gamma_i^E / (\Gamma_i^T + \Gamma_i^E)$ and $(1 - p_i) = \Gamma_i^T / (\Gamma_i^T + \Gamma_i^E)$ refer to the "weights" with which the local and thermalized baths contribute to the overall dynamics. The information about these weights can be obtained from Eq. (18). The parameters, p_i, Γ_i^T and Γ_i^E will generally depend on the layer. Indeed, for the lowest layer consisting of hydrogen atoms, p_1 should be close to unity because each hydrogen stands far from the equilibrated bath and has only one bond with the next layer. For the highest layer, p_N is close to zero because that layer is directly connected to the equilibrated bath. Note also that these parameters can correlate with the mode ω_{0i} chosen for a particle of the ith layer.

In Sec. II B we first solve the one-mode iLE of Eq. (34) and then show how other modes can be reintroduced into the theory. We concentrate on finding the effective temperature T_i^* of layer i, which, by analogy to Refs. 23 and 24, corresponds to the average kinetic energy of the particle:

$$T_i^* \equiv k_B^{-1} m_i \langle v_i^2 \rangle. \tag{35}$$

This temperature is time-dependent because the kinetic energy of the system is not stationary, as has been discussed above. The model described here can be treated as a coarse-grained form of the so-called Frenkel–Kontorova–Tomlinson (FKT) model[38,39] widely used in the theory of friction dynamics (see Refs. 40 and 41 and references therein).

B. The steady-state solution of one-mode iLE

Analytic manipulation of the stochastic equation (34) by use of Itō's formula and averaging over the stochastic noise, leads to differential equations for the first and second moments (for the sake of simplicity we omit below the indices i meaning that all the variables and parameters belong to the same layer):

$$\frac{d}{dt}\langle x \rangle = \langle v \rangle, \tag{36a}$$

$$\frac{d}{dt}\langle v \rangle = -\omega_0^2 \langle x \rangle + f(t) - \gamma \langle v \rangle, \tag{36b}$$

$$\frac{d}{dt}\langle x^2 \rangle = 2\langle xv \rangle, \tag{36c}$$

$$\frac{d}{dt}\langle xv \rangle = f(t)\langle x \rangle - \omega_0^2 \langle x^2 \rangle - \gamma \langle xv \rangle + \langle v^2 \rangle, \tag{36d}$$

$$\frac{d}{dt}\langle v^2\rangle = 2f(t)\langle v\rangle + \alpha\gamma\, p\,\omega_0^2\langle x^2\rangle - 2\omega_0^2\langle xv\rangle - (2(1-p)+\alpha p)\gamma\langle v^2\rangle + 2\gamma(1-p)k_{\mathrm{B}}T/m. \tag{36e}$$

Although this system can easily be solved numerically (as reported in Sec. IV), we first concentrate on the analytical solution at long times, when steady-state equilibrium is reached. The first two differential equations are well known as the equations of motion for the damped harmonic oscillator. Their solution at large times acquires the form

$$\langle x(t)\rangle = \frac{1}{\kappa}\left(F_0 + F_1\Re\frac{-i\omega_0^2\exp(i\omega t)}{\omega_0^2-\omega^2+i\gamma\omega}\right), \tag{37a}$$

$$\langle v(t)\rangle = \frac{F_1}{m}\,\Re\frac{\omega\exp(i\omega t)}{\omega_0^2-\omega^2+i\gamma\omega}, \tag{37b}$$

which can be used to specify the last three Eqs. (36c)–(36e) of the system. These equations, in matrix form, read

$$\frac{d}{dt}\mathbf{R}(t) = \hat{\mathbf{L}}\mathbf{R}(t) + \mathbf{U}(t), \tag{38}$$

where

$$\mathbf{R} = \begin{pmatrix}\langle x^2\rangle\\ \langle xv\rangle\\ \langle v^2\rangle\end{pmatrix}, \quad \mathbf{U}(t) = \begin{pmatrix}0\\ f(t)\langle x(t)\rangle\\ 2f(t)\langle v(t)\rangle + 2\gamma(1-p)k_{\mathrm{B}}T/m\end{pmatrix}, \quad \hat{\mathbf{L}} = \begin{pmatrix}0 & 2 & 0\\ -\omega_0^2 & -\gamma & 1\\ \alpha\gamma\, p\,\omega_0^2 & -2\omega_0^2 & -(2(1-p)+\alpha p)\gamma\end{pmatrix}.$$

In the steady-state regime the vector $\mathbf{R}$ is a linear response to the perturbations caused by $\mathbf{U}(t)$. Due to the fact that $\mathbf{U}(t)$ can be presented as a sum of harmonic terms,

$$\mathbf{U}(t) = \Re(\mathbf{U}_0 + \mathbf{U}_1 e^{i\omega t} + \mathbf{U}_2 e^{2i\omega t}),$$

the solution to Eq. (38) is a Fourier series of the form

$$\mathbf{R}(t) = \Re[-\hat{\mathbf{L}}^{-1}\mathbf{U}_0 + (i\omega - \hat{\mathbf{L}})^{-1}\mathbf{U}_1 e^{i\omega t} + (2i\omega - \hat{\mathbf{L}})^{-1}\mathbf{U}_2 e^{2i\omega t}]. \tag{39}$$

The first term in Eq. (39) is the stationary part of the solution— i.e., the solution averaged over the period of the oscillating force. Such quantities will be denoted as $\overline{\mathbf{R}}$. For the kinetic energy it gives

$$\frac{k_{\mathrm{B}}\overline{T}^*}{2} \equiv \frac{1}{2}m\overline{\langle v^2\rangle} = \frac{k_{\mathrm{B}}T}{2} + \frac{F_0^2}{4m(1-p)} \times\left[\frac{\alpha(u)\,p}{\omega_0^2} + \frac{\frac{1}{2}\alpha(u)\,p\left(\omega_0^2-\omega^2(u)\right)+\omega^2(u)}{\left(\omega_0^2-\omega^2(u)\right)^2+\gamma^2\omega^2(u)}\right]. \tag{40}$$

The second term on the RHS of this equation reflects the excitation effect caused by the periodic force $F(t)$. It is resonant by its nature, and its generalization for the multimode system is obvious: one needs to sum up over the harmonics of the perturbing force and average over the vibration spectrum $\rho(\omega_0)$ of a particular atom.

The friction force is found from the energy dissipation,

$$F_{\mathrm{fr}}u = \overline{F(t)\langle v(t)\rangle}. \tag{41}$$

Substitution of the force from Eq. (28) and steady-state velocity from Eq. (37b) and averaging over the period $2\pi/\omega$ gives

$$F_{\mathrm{fr}}u = \frac{F_0^2}{2m}\frac{\omega(u)^2\gamma}{\left(\omega^2(u)-\omega_0^2\right)^2+\gamma^2\omega^2(u)}. \tag{42}$$

This is a standard result for the linearized equations of motion[27,42] in the case of a single particle mode, but is not of practical use in our system with "mixed" coordinates. To generalize Eq. (42), the horizontal (sliding) and vertical modes should be considered separately, the integration over the vibration spectrum should be performed and higher harmonics of the perturbing force should be added. Note that the resulting friction force is expressed via the square amplitude of the perturbation, in accordance with the quadratic character of the RHS of Eq. (41): it is a product of a disturbance and a linear response to the disturbance. As Amontons' law states, the friction force between two solid surfaces is proportional to the load and, thus, $F_{\mathrm{load}} \sim F_{\mathrm{fr}} \sim F_0^2$. In the next section we show that this relation holds well in the simulations of Ref. 24 and the present one-mode iLE approach.

IV. NUMERICS FOR A NANOROD SLIDING ACROSS A SURFACE

Hase and co-workers[24] have used molecular dynamics simulations to describe the heat flows of a nanorod dragged across a surface. Specifically, heat flows from a surface of hydroxylated α-Al_2O_3 layers through a nanorod consisting of a small number of layers of the same material to an external thermalizing body at the top of the nanorod. Each such layer further splits into three layers consisting of H, O, and Al atoms, respectively. The theory developed above is not fully predictive because the parameters must be specified to the particular system. Nevertheless, once the parameters are specified, several of the features of the dynamics of the heat flow previously observed can be unified as is done here.

A. Model parameters

The effective friction coefficient is chosen to be $\gamma \approx 7.7 \times 10^{12}\,\mathrm{s}^{-1}$ for all the layers even though there exists at least three classes of layers corresponding to Al, O, or H. This

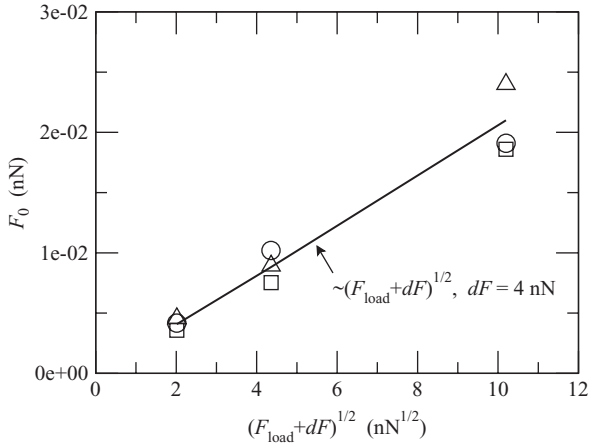

FIG. 2. The amplitudes F_0 of the excitation force (28) at different values of the loading force F_{load} for the first three sublayers: H-atom layer (circles), first O-atom layer (squares) and first Al-atom layer (triangles). The solid line is obtained through a least-squares fit of all nine data points.

simplification is based on the results presented in Figs. 3 of Ref. 24. They find that the relaxation of different atoms in any given layer toward the steady-state regime occurs on the same time scale. (See also Fig. 5 and discussion in the text below).

The "weight" p splits the action of friction into two parts: (i) $p\gamma$ which represents the "horizontal" coupling with the neighboring atoms and (ii) $(1-p)\gamma$ which corresponds to the friction caused by the global (phonon) bath. Although the parameter p is chosen empirically, it reflects an overall trend: The higher the layer, the stronger its connection to the thermal bath, in accordance with Eq. (18) (see Table I).

The characteristic frequencies ω_{0i} for the layers are listed in Table I. The oscillations of the hydrogen atoms are slower when calculated directly from the force field:[22] $\omega_{O\text{-}H} \approx 7 \times 10^{14}\,\mathrm{s}^{-1}$ for the O–H stretch and $\omega_{O-H-Al} \approx 9 \times 10^{13}\,\mathrm{s}^{-1}$ for the H–O–Al bend. As these frequencies are the highest ones in the system, the contribution of other modes lower the effective frequency of the hydrogen layer. This effective frequency can thus be treated as a geometric mean of the frequency distribution corresponding to the thermodynamics of a crystal lattice at high temperatures.[25]

The effective vibrational frequencies ω_{0i} for the other two layers are scaled according to mass ratios. For example, the effective frequency for the effective oxygen-layer particle is taken to be $\omega_{0O}^2 = (m_H/m_O)\,\omega_{0H}^2$. This is a reasonable assumption because the effective force constants for each layer are approximately of the same value, and hence the predominant variation in the frequencies is due to mass ratios. Regardless, these frequencies are close to each other and are of the order of standard Debye value which can be estimated as $\sim 10^{12}$–$10^{13}\,\mathrm{s}^{-1}$ for the speed of sound, $c \sim 1000$ m/s. The effective frequencies ω_{0i} and the friction coefficient γ are of the same order of $10^{13}\,\mathrm{s}^{-1}$ corresponding to the choice of the surface parameters used also in Ref. 43.

The force amplitudes F_{0i} are fitted independently for each value of the load, F_{load}, and for each layer. These amplitudes are illustrated in Fig. 2. They are indifferent to the sliding velocity and do not exhibit any dependence on the particular layer i. This observation can be explained by noting that the force applied to the edge of the spring chain is distributed uniformly along the chain causing the same tension on each spring. According to Fig. 2, there exists a simple relationship between the force amplitudes F_{0i} and the load force F_{load}. This relationship is quadratic by its nature, as in Eqs. (40) and (42), but implies that there is a shift in the load equal to 4 nN. This additional load is related to the adhesive interaction between the two surfaces in accordance with observations in Ref. 24. The quadratic connection of F_{0i} to the load and friction forces, F_{load} and F_{fr}, make them linearly coupled with each other, in accordance with Amontons' first law of friction.

B. Relaxation at small velocities

The partitioning of energy according to the variable u_0 in Eq. (32) has been introduced to account for the appearance of "concerted" equilibration at low velocities. In this regime, atoms at the upper surface relax within the centers of their potential wells in between interactions with the lower surface. When the upper and lower surface atoms overlap, there is a sizable coherent interaction that induces a concerted kick on the surface atoms. Their kinetic energy increases momentarily and this is subsequently dissipated by the environment. However, the energy stored in the potential form between releases does not excite the neighboring atoms. The phenomenological function $\alpha(u)$ defined in Eq. (32) cancels out this transient contribution of the potential energy at very slow sliding.

The threshold sliding velocity u_0 is found by fitting the velocity dependence of the steady-state temperature $\overline{T}^*$ in Eq. (40) to the data shown in Fig. 6 of Ref. 24 (this figure is reproduced as Fig. 4 below). The values of u_0 shown in Table I are about $10^{-5}\,c$ where $c \sim 1000$ m/s is the speed of sound. It is much smaller than the transition between stick-slip and sliding regimes[20] which is about $u_{tr} \sim 10^{-2}\,c$. It can be attributed to the velocity at which the stick-slip regime is fully established. The function $\alpha(u)$ in Eq. (32), thus interpolates the region between u_0 and u_{tr}.

Analysis of Eq. (40) shows that the critical value of u, at which the turn-over of the steady-state temperature $\overline{T}^*$ can be observed, is

$$u_{tr} \sim \left(p u_0 \omega_0^2 a^2 / (4\pi)^2\right)^{1/3}, \tag{43}$$

if ω_0 and γ are of the same order, as in our case. Because $c \approx a\omega_0/(2\pi)$, this expression can be recast as

$$u_{tr}/c \sim (p u_0/c)^{1/3}, \tag{44}$$

which takes on values in the range $(10^{-2}$–$10^{-1})$, with the parameters taken from Table I. Therefore, the values of u around 10 m/s divide the stick-slip and the smooth sliding regimes, as expected (see Fig. 4). Note also that nonzero value of u_{tr} in Eqs. (43) and (44) is possible only if $p \neq 0$, i.e., if the local (horizontal) bath concurrently contributes to the dynamics. As it is shown in Table I, p is close to unity.

Thus the smooth sliding regime does not immediately follow the stick-slip one: there is a velocity gap which exhibits a dual regime behavior. Equation (44) marks the tran-

TABLE II. Ratios of heat transfer coefficients used in Fig. 3.

F_{load}	25 (nN)	100 (nN)
$D_{H,O}/D_{O,Al}$	0.045	0.098
Ω_i/ω_{0i}	7.6	4.2

sition between these regimes in the framework of the present approach.

C. Smoothed temperature profile

In Fig. 3, two profiles of the steady-state averaged temperature as calculated through Eq. (18) are compared against the data reproduced from Fig. 5 in Ref. 24. As remarked in Sec. II B, the relative values of the heat transfer coefficients fully define the temperature profiles. The coefficients for the O and Al layers, $D_{O,Al}$ and $D_{Al,O}$, are equal to each other due to the symmetry of Eq. (16) with respect to the permutation of indexes, but differ from $D_{H,O}$. The latter is much lower owing to the higher vibration frequency of hydrogen atoms (Table II).

The frequencies and friction coefficients from Table I are used to estimate the ratios of $D_{H,O}$ and $D_{O,Al}$ from Eq. (16). The quantities Ω_i, representing the frequencies for the corresponding interlayer interactions, must also be estimated. Assuming that the square of these frequencies are inversely proportional to particles masses, we found them to be several times larger than the analogous ω_{0i} (see Table II). This suggests that the effective interaction between the particles belonging to adjacent layers must include interactions to the surrounding atoms so as to adequately describe the temperature profiles in the heat transfer coefficients.

D. Smoothed temperature versus sliding velocity

The dependence of the stationary values of the effective temperature $\overline{T}^*$—calculated from Eq. (40)—on the sliding velocity u are shown in Fig. 4 for different layers at various loads. The one-mode model exhibits very good agreement with the molecular dynamics simulations of Ref. 24. The only discrepancy in the forms of the curves can be seen at weak loads, F_{load} near 0.0625 nN, but the temperature ranges remain in good agreement even in this case.

The case for which $\alpha(u) \equiv 1$ (or $u_0 = 0$)—i.e., when the local temperature is associated with the full energy— is shown in the upper panel as dotted lines. As shown, the deviation of $\alpha(u)$ from unity leads to a decrease in the steady-state temperature level at slow sliding, $u < 10$ m/s, approximately when the transition to the stick-slip regime is observed.

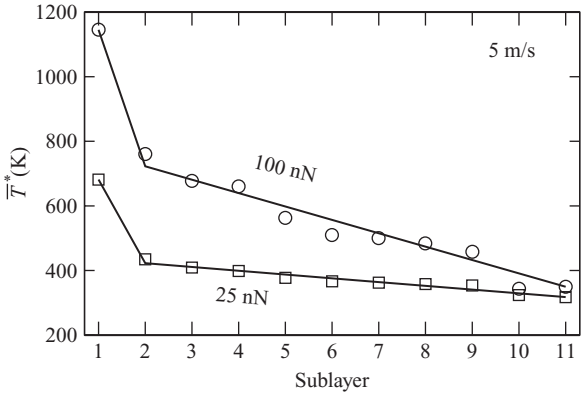

FIG. 3. Effective temperature $\overline{T}^*$ of the upper surface sublayers at sliding velocity $u = 5$ m/s and different load: 100 nN (circles) and 25 nN (squares). Sublayers 1–3 are three lowest interfacial layers of H, O, and Al atoms, respectively. The simulation data (symbols) are adapted from Ref. 24.

E. Time dependence of the temperature

Numerical solutions for the differential equation (38) with parameters taken from Table I and Fig. 2 are shown in Fig. 5. The steady-state regime is established during the time needed to slide over a couple of interatomic distances in the case of fast sliding (the upper panel), whereas at slower sliding it occurs significantly earlier (the lower panel), in accordance with Ref. 24 (see Fig. 3 therein). The amplitudes of the temperature oscillations also exhibit a good agreement with those found in Ref. 24: in the upper panel only the lower limit for Al-atom temperature is raised by 50 K; in the lower panel maximal values for H-atom and O-atom data are increased by about 100 K, and the minimal values of Al-atom temperature are raised by 50 K.

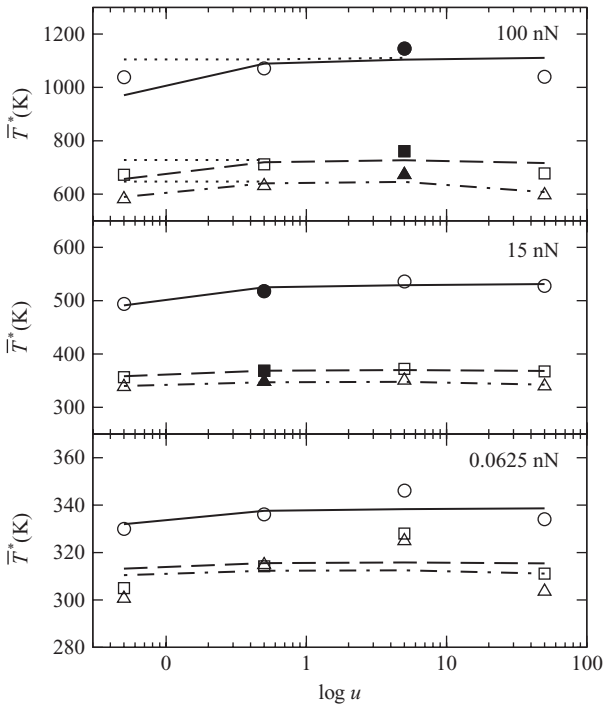

FIG. 4. The steady-state effective temperature, $\overline{T}^*$, vs logarithm of the sliding velocity in m/s for different values of the load: 100 nN (upper panel), 15 nN (middle panel) and 0.0625 nN (lower panel). Symbols show the results of MD simulations (Ref. 24) for the first three sublayers: H-atom layer (circles), first O-atom layer (squares) and first Al-atom layer (triangles). Filled symbols correspond to the parameter sets for which the sliding dynamics of the effective temperature is calculated in Fig. 5. Solid lines are the results of the stochastic model[Eq. (40)]. Dotted lines in the upper panel are calculated at $\alpha \equiv 1$ [Eq. (32)]. The simulation data are adapted from Ref. 24.

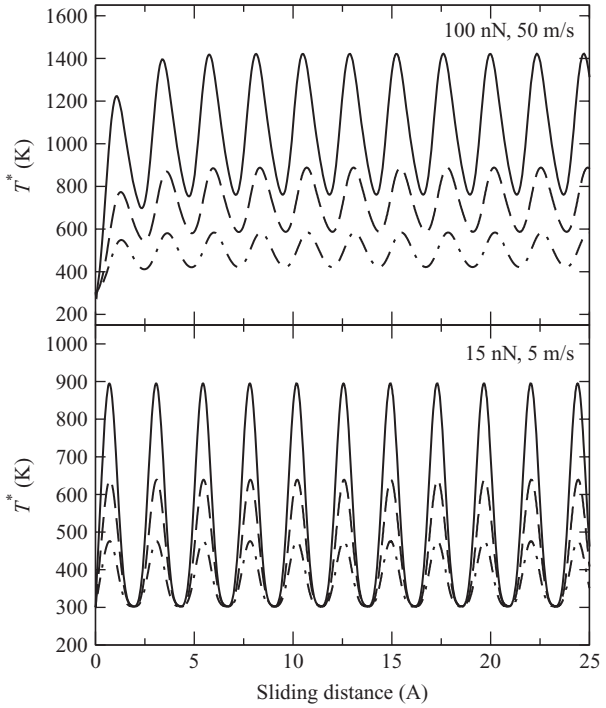

FIG. 5. The effective temperature, T^*, vs sliding distance obtained from the numerical solution of Eq. (38): for the H-atom layer (solid curve), first O-atom layer (dashed curve) and first Al-atom layer (dash-dotted curve). Upper panel: $F_{\text{load}} = 100$ nN, $u = 50$ m/s. Lower panel: $F_{\text{load}} = 15$ nN, $u = 5$ m/s.

V. CONCLUDING REMARKS

The iLE-based approach has been used to investigate the nonequilibrium temperature distribution along different atomic layers of a nanorod sliding across a surface. The generalization of the Langevin approaches available from the iLE framework is essential because it can account for nonstationary environments. This advantage is exploited here in representing the response of the complex bath using two subenvironments: a global equilibrium one maintained at a constant temperature and a local nonequilibrium one. The collective oscillations of the layers are represented by the motion of effective atoms immersed in this structured environment.

In the framework of the model, the oscillations associated with the dragging process are caused by the periodic force acting on the generalized atomic coordinates. The temperature of the local bath for each layer is defined via the average total energy of a representative oscillator—viz. the effective atoms. Such an approximation is good in the case of smooth-sliding as seen at large thermal velocities, whereas in the stick-slip regime an alternative mechanism is required. In this very slow dragging regime, the coordinates of the particles are fully relaxed within their potential energy minima periodically and coherently. The transient energy kick must be suppressed in order to obtain steady-state local temperatures which are in turn primarily determined by the kinetic part of the oscillation. Thus the coherence of the heat flow through the nanorod is highly dependent on the relative decoherence of the energy into the layer. This, in turn, suggests that the heat flows would be altered in cases when the nanorod layers are reduced to dimensions that are small enough to structure their dissipative response.

By comparison with recent simulations of the friction process between two alumina surfaces,[24] it has been shown that the model adequately captures the time-dependent and steady-state properties of the heat flows through a nanorod. Thus, the origin of the temporal temperature oscillations corresponds to that described in Ref. 24: being synchronous with the periodic force, the temperature acquires its maximum and minimum at the moments when the upper surface is at minimum and maximum of the potential energy describing the contact. Note also that a nanorod consisting of several layers is so small that all the oscillations are, in fact, coherent.

Another interesting effect is the relaxation time needed for establishing the steady-state regime of these oscillations. In accordance with Fig. 3 of Ref. 24, at the dragging speed 50 m/s the system relaxes until the sliding distance becomes around 2–3 Å. This process takes approximately 10^{-12} s. At a slower dragging speed, 5 m/s, the relaxation period is not visible due the shortness of the sliding distance. Within the framework of the iLE approach (Fig. 5), this effect can be fully interpreted as resulting from the decoherence time of the bath response and quantified by the friction coefficient, γ. The values of the latter relevant to this system have been estimated through the present theory and detailed in Table I.

The large drop in the temperature T^* from the first to second sublayers in Fig. 3 is attributed to a much lower heat transfer coefficient between the H and O layers (due to the loose connection of peripheral hydrogen atoms) as compared with O–Al heat transfer coefficient; see Table II. However, following Eq. (18), this effect becomes less pronounced for a thicker nanorod. A thick rod also gives a smoother temperature profile in a better agreement with Fourier's law. The amplitudes of the temperature oscillations should be lower for a larger system. The reason for this lies in the decreased coherence of the oscillations of effective coordinates (Sec. II C) due to (i) increased damping caused by a much more massive bath of equilibrated lattice vibrations, and (ii) a large amount of layers involved in the process; indeed, the phase shifts between them cannot be neglected and lead to the averaging of phases.

In summary, the nontrivial coherences in the nature of the heat flows through a layered nanorod can be accurately included using a reduced-dimensional model with a dimension that is commensurate with the small and finite number of layers of the nanorod. This provides a significant simplification in comparison to all-atom models which account for all the particles in all three degrees of freedom. The accuracy of this reduced-dimensional model will break down as the nanorod layers become small and finite such that their response becomes nonuniform. Nevertheless, the present model should be helpful in assessing when heat build-ups might give rise to defects in the nanorod and which layers will be most prone to those defects. For example, the size of the temperature drop from the first to second sublayers will determine how many of these layers are above the melting temperature of the lattice.

ACKNOWLEDGMENTS

This work has been partially supported by the National Science Foundation through Grant No. CHE 0749580, and by the Air Force Office of Scientific Research through Grant No. FA9550-09-1-0597.

[1] S. Zilberman, B. N. J. Persson, and A. Nitzan, J. Chem. Phys. **115**, 11268 (2001).
[2] S. Zilberman, T. Becker, F. Mugele, B. N. J. Persson, and A. Nitzan, J. Chem. Phys. **118**, 11160 (2003).
[3] F. Yin, D. Bedrov, G. D. Smith, and S. M. Kilbey II, J. Chem. Phys. **127**, 084910 (2007).
[4] I. E. Castelli, R. Capozza, A. Vanossi, G. E. Santoro, N. Manini, and E. Tosatti, J. Chem. Phys. **131**, 174711 (2009).
[5] Y. He, S. Chen, J. C. Hower, M. T. Bernards, and S. Jiang, J. Chem. Phys. **127**, 084708 (2007).
[6] D. B. Knorr, Jr., T. O. Gray, and R. M. Overney, J. Chem. Phys. **129**, 074504 (2008).
[7] J. N. Glosli and G. M. McClelland, Phys. Rev. Lett. **70**, 1960 (1993).
[8] J. Harrison, C. White, R. Colton, and D. Brenner, Phys. Rev. B **46**, 9700 (1992).
[9] J. A. Harrison, R. J. Colton, C. T. White, and D. W. Brenner, Wear **168**, 127 (1993).
[10] J. A. Harrison, C. T. White, R. J. Colton, and D. W. Brenner, Thin Solid Films **260**, 205 (1995).
[11] M. D. Perry and J. A. Harrison, J. Phys. Chem. **99**, 9960 (1995).
[12] M. D. Perry and J. A. Harrison, Langmuir **12**, 4552 (1996).
[13] J. Zhang and J. Sokoloff, Phys. Rev. E **71**, 066125 (2005).
[14] O. A. Mazyar and W. L. Hase, J. Phys. Chem. A **110**, 526 (2006).
[15] U. Wyder, A. Baratoff, E. Meyer, L. N. Kantorovich, J. David, S. Maier, T. Filleter, and R. Bennewitz, J. Vac. Sci. Technol. B **25**, 1547 (2007).
[16] M. T. Knippenberg, P. T. Mikulski, B. I. Dunlap, and J. A. Harrison, Phys. Rev. B **78**, 235409 (2008).
[17] J. A. Harrison, J. D. Schall, M. T. Knippenberg, G. Gao, and P. T. Mikulski, J. Phys. Condens. Matter **20**, 354009 (2008).
[18] A. Martini, Y. Dong, D. Perez, and A. F. Voter, Tribol. Lett. **36**, 63 (2009).
[19] Y. Liao and L. Marks, Tribol. Lett. **37**, 283 (2010).
[20] O. Braun and A. Naumovets, Surf. Sci. Rep. **60**, 79 (2006).
[21] D. J. Mann and W. L. Hase, Tribol. Lett. **7**, 153 (1999).
[22] D. J. Mann, L. Zhong, and W. L. Hase, J. Phys. Chem. B **105**, 12032 (2001).
[23] H. Xie, K. Song, D. J. Mann, and W. L. Hase, Phys. Chem. Chem. Phys. **4**, 5377 (2002).
[24] O. A. Mazyar, H. Xie, and W. L. Hase, J. Chem. Phys. **122**, 094713 (2005).
[25] L. D. Landau and E. M. Lifshitz, *Course of Theoretical Physics: Statistical Physics, Part 1* (Butterworth-Heinemann, Oxford, 1980).
[26] A. M. Kosevich, *The Crystal Lattice: Phonons, Solitons, Dislocations, Superlattices* (Wiley-VCH, Berlin, 1999).
[27] J. B. Sokoloff, Phys. Rev. B **42**, 760 (1990).
[28] R. Hernandez and F. L. Somer, J. Phys. Chem. B **103**, 1064 (1999).
[29] R. Hernandez and F. L. Somer, J. Phys. Chem. B **103**, 1070 (1999).
[30] A. V. Popov, J. Melvin, and R. Hernandez, J. Phys. Chem. A **110**, 1635 (2006).
[31] A. V. Popov and R. Hernandez, J. Chem. Phys. **131**, 024503 (2009).
[32] A. V. Popov and R. Hernandez, J. Chem. Phys. **126**, 244506 (2007).
[33] M. M. Millonas and C. Ray, Phys. Rev. Lett. **75**, 1110 (1995).
[34] J. R. Chaudhuri, G. Gangopadhyay, and D. S. Ray, J. Chem. Phys. **109**, 5565 (1998).
[35] J. Hohlfeld, S. Wellershoff, J. Güdde, U. Conrad, V. Jähnke, and E. Matthias, Chem. Phys. **251**, 237 (2000).
[36] F. Zamponi, F. Bonetto, L. F. Cugliandolo, and J. Kurchan, J. Stat. Mech.: Theory Exp. P09013 (2005).
[37] E. Hershkovits and R. Hernandez, J. Phys. Chem. A **105**, 2687 (2001).
[38] Y. Frenkel and T. Kontorova, Phys. Z. Sowjetunion **13**, 1 (1938).
[39] T. Kontorova and Y. Frenkel, Zh. Eksp. Teor. Fiz. **8**, 89 (1938).
[40] E. Meyer, T. Gyalog, R. M. Overney, and K. Dransfeld, *Nanoscience: Friction and Rheology on the Nanometer Scale* (World Scientific Publishing Company, Inc., Singapore, 2002).
[41] O. M. Braun and Y. S. Kivshar, *The Frenkel-Kontorova Model: Concepts, Methods, and Applications* (Springer-Verlag, Berlin, 2004).
[42] M. Weiss and F.-J. Elmer, Z. Phys. B **104**, 55 (1997).
[43] M. Shugard, J. C. Tully, and A. Nitzan, J. Chem. Phys. **66**, 2534 (1977).